Tribol Lett (2013) 49:117–125
DOI 10.1007/s11249-012-0045-2

ORIGINAL PAPER

Friction Properties of Lubricated Laser-MicroTextured-Surfaces: An Experimental Study from Boundary- to Hydrodynamic-Lubrication

Michele Scaraggi · Francesco P. Mezzapesa · Giuseppe Carbone · Antonio Ancona · Luigi Tricarico

Received: 13 June 2012 / Accepted: 15 September 2012 / Published online: 4 October 2012
© Springer Science+Business Media New York 2012

Abstract We present measurements of friction coefficient of lubricated laser surface textured (LST) microstructures with two different geometries. The former is made of a square lattice of microholes; the latter is constituted by a series of microgrooves. We analyze sliding velocities spanning more than two orders of magnitude to cover the entire range from the boundary to the hydrodynamic regime. In all cases, the interfacial pressure is limited to values (relevant to particular manufacturing processes) which allow to neglect macroscopic elastic deformations, piezo-viscosity and oil compressibility effects. The measured Stribeck curves data are compared with those obtained for the flat control surface and show that the regular array of microholes allows to reduce friction over the entire range of lubrication regimes with a decrease of about 50 % in the hydrodynamic regime. On the contrary, the parallel microgrooves lead to an increase of friction compared to the flat control surface with a maximum increase of about 80–100 % in the mixed lubrication regime. These remarkably opposite friction results are then explained with the aid of numerical simulations. Our findings confirm that LST may have cutting edge applications in engineering, not only in classical applications (e.g., to reduce piston-ring friction losses in internal combustion engines) but also, in particular, in technological processes, such as hydroforming, superplastic forming, where the mapping of the frictional properties of the mold has a crucial role in determining the final properties of the mechanical component.

Keywords LST · Surface texturing · Laser ablation · Friction · Bearings · Lubrication

1 Introduction

Nowadays it is widely recognized that introducing a deterministic, or even statistic, pattern of chemical/physical discontinuities on the surface of interacting components may significantly affect the overall properties of the contact, such as friction, adhesion, and wear [1–12]. A consequence of this is the remarkable number of developed applications, ranging from life science (e.g., cell adhesion/proliferation, tissue engineering, and tactile perception) to engineering (e.g., microfluidics, superhydrophobic surfaces, bio-inspired textured surface, seals, surface structuring for manufacturing tools, and bearings) [13]. By restricting the field to machine elements and manufacturing tools, an increasing amount of research is currently devoted to the experimental and theoretical investigation of the effects of surface lattice microstructuring on the frictional and wear properties of the contact with particular (growing) attention to laser surface texturing (LST). Indeed, recent technological improvements in LST, which allowed a considerable reduction of surface (and subsurface) cracks' formation and residual stresses, have ranked top such a micromanufacturing process in terms of ease and low costly working with respect to other common processes, such as ion beam, etching techniques, etc. [8]. This has been obtained by employing fiber laser systems with femto- and pico-second pulse duration at frequencies of

M. Scaraggi (✉)
DII, Universitá del Salento, 73100 Monteroni-Lecce, Italy
e-mail: michele.scaraggi@unisalento.it

F. P. Mezzapesa · A. Ancona
CNR-IFN UOS Bari, Via Amendola 173, 70126 Bari, Italy

G. Carbone · L. Tricarico
DMMM, Politecnico di Bari, V.le Japigia 182, 70126 Bari, Italy

www.manaraa.com

several kHz. As a result, high-aspect-ratio/high-density structures of microholes can be successfully fabricated over steel and copper, where fast energy deposition and negligible heated zones are guaranteed at such laser material interaction timescales [14].

A decade of experimental (and theoretical) research on microstructuring lubrication has shed light on the positive effect, that an artificial surface texturing *may* have on enhancing the load capacity, wear resistance, and friction coefficient of mechanical components [8, 9, 13] and manufacturing tools [12]. In the case of total texturing, conformal contacts have been investigated in a number of interesting experimental studies. In particular, Kovalchenko et al. [15] first reported on the transition from the boundary to the hydrodynamic regime in the case of a texture constituted by a lattice of circular holes, whereas Galda et al. [16] and Vilhena et al. [17] discussed, respectively, the effect of hole shape and laser working parameters on the Stribeck curve. Texturing hydrodynamics has been also investigated in practical cases, e.g., for totally-textured rings [18] and partially-textured thrust bearings [19, 20] and piston rings [21] showing, on the experimental basis, both a remarkable friction reduction due to the microdimpled geometry, and the existence of optimal texturing for larger load support capabilities. Literature also reports on detailed experimental investigations in the case of grooved microgeometries, see, e.g. Refs. [22–24]. In particular, under lubricated reciprocating sliding motion, Yuan et al. [22] discussed the effect of the groove inclination angle (the angle between the sliding direction and the microchannel path) on the contact friction. The authors found, as expected, no preferential inclination angle able to minimize the friction at the different investigated applied loads. However, friction for the grooved surface resulted usually lower than the corresponding value for the untextured case, a result not always confirmed in literature (we suppose as a consequence of the rather one-dimensionality of the contact geometry). Indeed, Adatepe et al. [23] have recently compared the friction of transverse and longitudinal grooved texture with the untextured case for the journal-bearing geometry, showing that the larger friction values were obtained for the transverse grooves over all the Stribeck curve, followed then by the longitudinal texture friction. The latter remarkable result suggests, together with the recent findings on dimpled texture [15], that the adoption of structural textures of different nature (i.e., circular/elliptical or grooved) may allow to (macroscopically) pointwise differentiate the frictional characteristics of the contact, a practice which would correspond to a step forward in technological applications, such as superplastic forming, where a mold friction mapping would be the optimal choice to optimize the working process and the finishing results of the working piece.

In this work, we provide our experimental contribution in the field of microstructured texturing lubrication, by carrying out a campaign focused on the determination of friction curves (Stribeck curves) on a range of sliding velocities covering more than two orders magnitudes, i.e., from the boundary to the hydrodynamic regime, under isoviscous rigid lubrication. We measure the coefficient of friction (COF), μ, in the case of two different texture geometries: (i) the former is constituted by a regular array of microholes, and (ii) the latter is made of a series of equally spaced parallel microgrooves. In particular, microhole textures lead to a strong reduction of COF, whereas microgrooves determine a friction increase. Numerical full-scale calculations are also presented and discussed to theoretically justify the experimental findings. Our results confirm LST as a potentially crucial tool to control (increase or decrease) the interfacial friction in processes, such as metal forming, where the local friction characteristics of the tool have a key role on determining the mechanical properties of the final product.

2 Experimental Setup Details

Friction measurements were carried out on a CSM High Temperature pin-on-disk Tribometer (THT), see Fig. 1a. The contact geometry has been redesigned to adopt larger sliding velocities compared to the standard equipment. The core of the system is constituted by a rotating sample disk in contact with a spherical cap, the latter being cut from a machine bearing 100Cr6 ball, Fig. 1b. The surface of the spherical cap is obtained with a series of successive sandpaper sweeps with decreasing particle size. The final mirror-finishing state is shown in Fig. 2, where the atomic force microscopy acquisition of the surface topography reveals the roughness of the finished sample surface (root-mean-square $h_{\mathrm{rms}} \approx$ 20 nm), characterized by nanometer-sized randomly directed scratches. The substrate is an aluminum alloy AA6061 sheet with $h_{\mathrm{rms}} \approx 0.6$ μm. The contact pair (disk and pin-end) is immersed in a lubricant bath, the temperature of which is constantly monitored during the test. The adopted lubricant is a pure mineral oil (Oroil Therm 7 from Orlando Lubrificanti S.r.l.) with dynamic viscosity $\eta = 0.0516$ Pa s at 50 °C. LST technique is employed to texture the surface of the spherical cap. In Fig. 3, we show a schema of the ablation setup. The source used for the laser microtexturing of high density patterns is a prototype ytterbium-doped fiber laser amplifier delivering 120-ps pulses at the wavelength of 1,064 nm. A maximum average pulse energy of about 90 μJ at 110 kHz repetition rate could be provided although only few tens of microjoules were needed to have good quality features with reduced generation of molten material and minimal thermal

www.manaraa.com

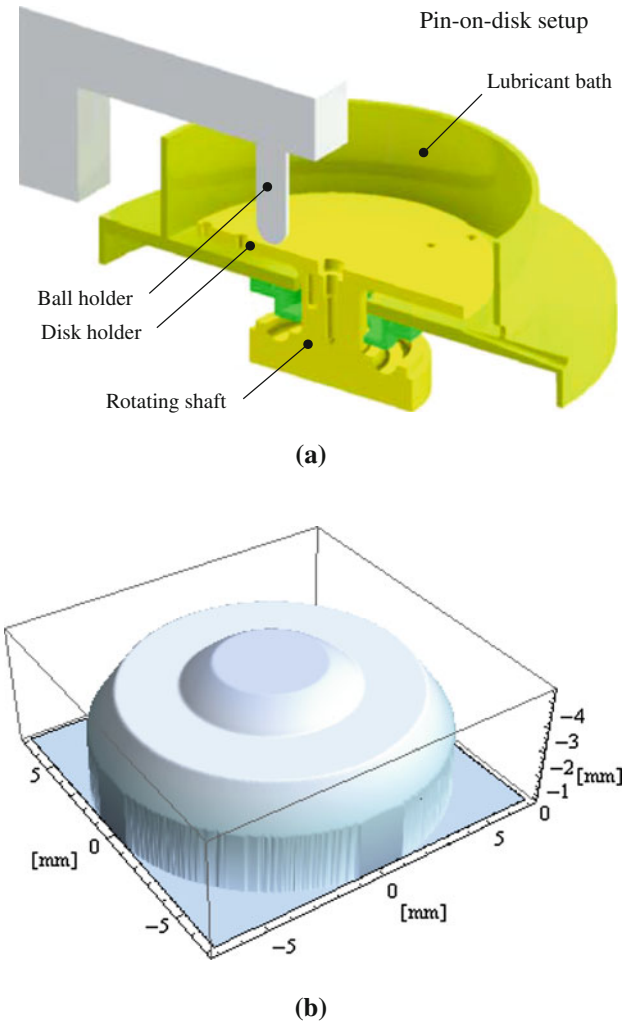

Fig. 1 Schema of the experimental setup employed to carry out the Stribeck curve measurements (**a**). The spherical cap obtained by the 100Cr6 steel ball mounted on the ball holder (**b**)

damage to the surrounding bulk material [25]. The linear polarization of the exit beam was converted into a circular one by using a quarter-wave plate to prevent anisotropic absorption inside the metal. The laser beam has been focused and moved on the sample surface using a galvanometric scanning system equipped with a 100-mm focal-length F-theta lens, which produced a focal spot diameter $\approx$20 μm. Preliminarily, microdrilling experiments were performed to adjust the working parameters to optimize the shape and the steepness of the drilled holes as well as the reproducibility of the process.

Several sets of microdimples (Fig. 4a) and -grooves (Fig. 4b) were realized by accurately scanning the focal spot on the target surface in the trepanning configuration. The average laser power was set at 1.25 W and the scan speed and number of loops were optimized at 1 mm/s and 75, respectively. In particular, in this work, we focus on two square lattices of circular microholes: (i) the CT1

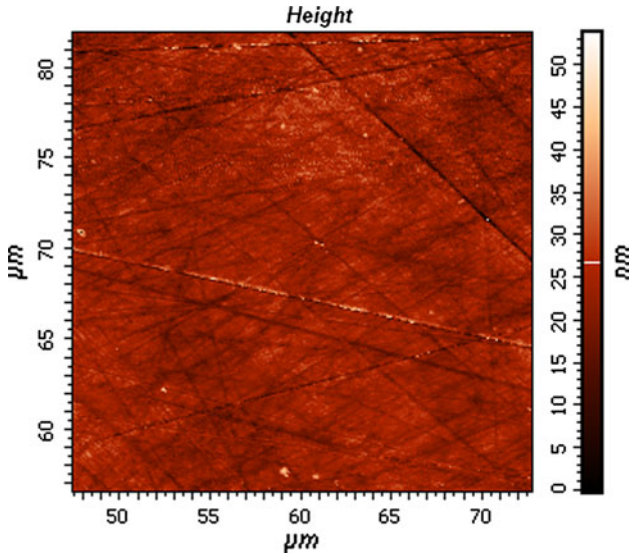

Fig. 2 Atomic force microscopy acquisition of the mirror-finished spherical cap sample. The surface root-mean-square roughness $h_{\mathrm{rms}} \approx 20$ nm. Scratches due to larger diamond particles are visible

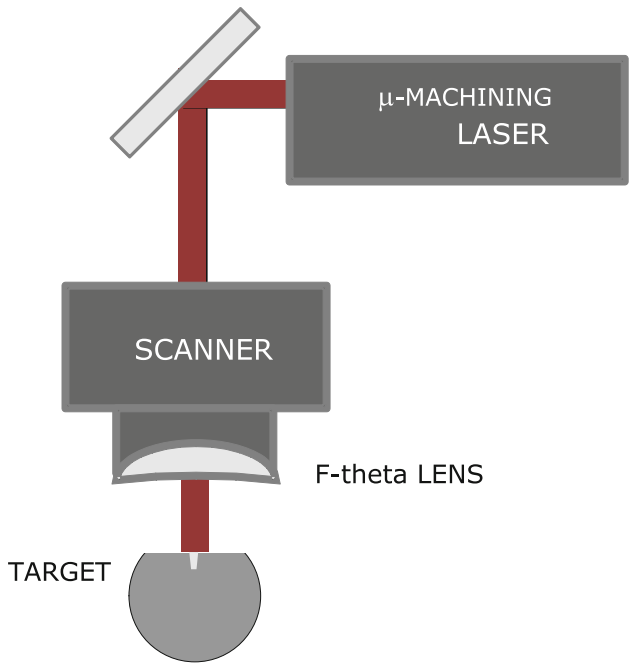

Fig. 3 The laser ablation experimental setup (schematic)

sample with hole diameter $d = 50$ μm, center to center distance $i = 100$ μm (void density $p_{\mathrm{h}} = 20$ %), and (ii) the CT2 sample with $d = 50$ μm, center to center distance $i = 75$ μm ($p_{\mathrm{h}} = 35$ %). We also consider (iii) a texture of parallel grooves with period spacing 100 μm, groove width 50 μm ($p_{\mathrm{h}} = 50$ %) in a transversal (GTt) (the sliding velocity is perpendicular to the grooves) and longitudinal (GTl) configurations. The ablation penetration, h_{d}, is kept fixed to a value $\approx$10 μm. No further polishing of the

www.manaraa.com

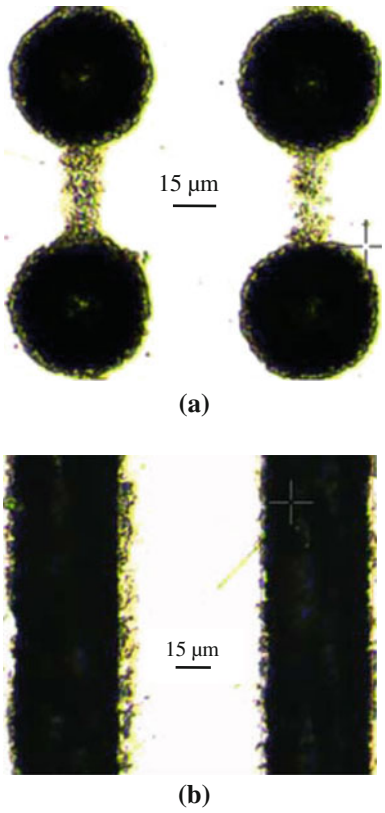

Fig. 4 Optical micrographs of the adopted texture geometry: a square lattice of circular holes (**a**); a texture of parallel grooves (**b**). The groove texture is defined longitudinal (transverse) when the sliding direction is parallel (perpendicular) to the grooves

Table 1 Steady sliding parameters

Normal load	2N
Nominal contact area	≈ 14 mm^2
Velocity range	0.01–1.2 ms^{-1}
Temperature	70 °C
Viscosity-temperature dependence	$\log \eta/\eta_0 = \sum_{k=1}^{3} a_k (t - t_0)^k$
	$\eta_0 = 1.51$Pa s, $t_0 = 0.01$ °C
	$a_1 = -7.58 \times 10^{-2}$, $a_2 = 2.82 \times 10^{-4}$
	$a_3 = -3.76 \times 10^{-7}$

textured surface was performed since the bulges around the rim of the texture border were comparable with the roughness present on the aluminum counter surface. The friction measurement conditions are reported in Table 1.

The test protocol was as follows. A single μ–ηU curve, where μ is the friction coefficient and η and U are, respectively, the oil viscosity and sliding velocity, is obtained using only one contact pair sample and new lubricant. Each (ηU, μ) point of the diagram was calculated by averaging five consecutive measurements (with temperature corrected viscosity). Given the value of the sliding speed, each measurement is carried out in two steps: during the first step the two surfaces are separated by a few hundred micrometers gap u to measure the resistance force f_d due to the action of the oil bath on the ball holder. Then, in the second step the two surfaces are left in contact and the resulting friction f_t is measured. The COF is then calculated as $\mu = f_t - f_d$, which is also a bias-free measure. After each set of measurements with the same lubricant, all the parts of the apparatus in direct contact with the lubricant have been washed with a copious amount of distilled water, followed by alternating use of isopropanol and acetone. Mobile parts are also washed for 15 min in a ultrasonic isopropanol bath.

3 Results and Discussion

In Fig. 5a, we show the (experimental) Stribeck curve of the control surface, compared with the hydrodynamics predictions for the smooth sliding geometry. Observe that there is a good agreement with the full film stage of the friction curve, which reveals a transition to the hydrodynamic lubrication above values of ηU close to 0.01 N/m. This is consistent with the film thickness predictions $u \approx 1\,\mu\text{m} \gtrsim h_{\text{rms}} = 0.6\,\mu\text{m}$ at which the transition is expected to occur, see Fig. 5b. Note in Fig. 5a that the adopted experimental protocol and tribo setup, allows to capture the full frictional behavior of the contact, i.e., from the boundary to the hydrodynamic regime with no loss of details. In Fig. 6, we show the fluid pressure field (in gray scale, normalized with respect to the maximum calculated pressure value $p_{\text{max}}^{\text{smooth}}$), and the cavitating area (red domain) as a function of the contact position, for the same contact parameters adopted in the calculation of Fig. 5b and for $h_{\text{min}} = 2\,\mu$m (the sliding direction is uniquely determined by the position of the cavitation area). The cavitation has been numerically handled, within the JFO model, with the adoption of the well-known cavitation index-based Reynolds lubrication equation; the latter solved with an error smoothing technique over multiple grid scales. Interestingly, despite the ideal conformity of the contact geometry, a pressure rise is generated at the contact inlet where an almost stepwise variation of the oil gap is encountered. This over pressure is then gradually decreasing toward the contact outlet, resulting in the formation of a cavitation zone which does not involve almost the whole conforming portion of the interaction domain. Hence, we can safely say that this flat-on-flat contact occurs under full film conditions for the untextured pair. The frictional shear stress field (in gray scale, normalized with respect to the value $\eta U/h_{\text{min}}$) is instead shown in Fig. 7. Observe that, as expected, the frictional

www.manaraa.com

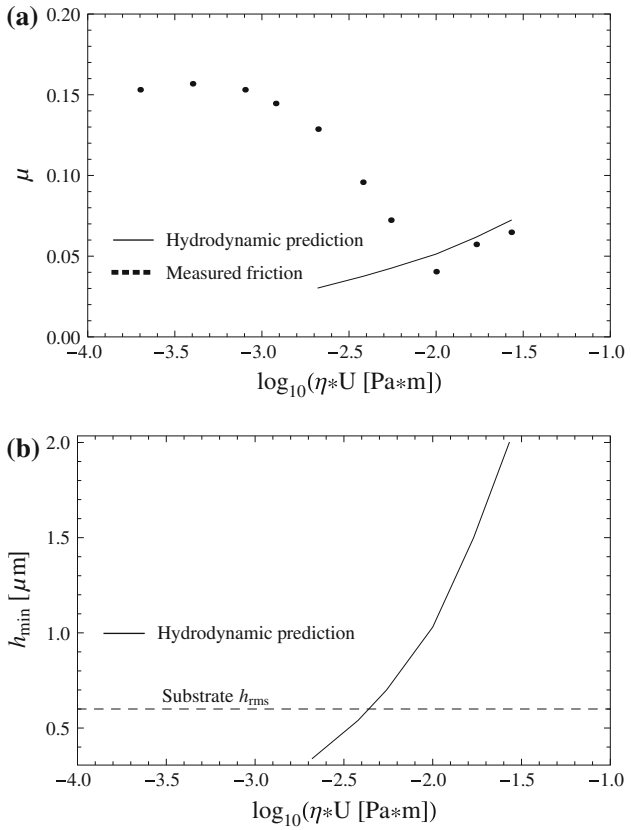

Fig. 5 The coefficient of friction μ as a function of the product ηU friction for the untextured surface. Measurements (*points*) and the hydrodynamic predictions (*solid line*) (**a**); the predicted central separation from simulations (**b**). Observe that the experimental points start to match the hydrodynamic theoretical predictions when $\eta U > 0.01$ N/m, i.e., when the predicted lubricant film thickness becomes comparable to the combined rms roughness of the contacting surfaces

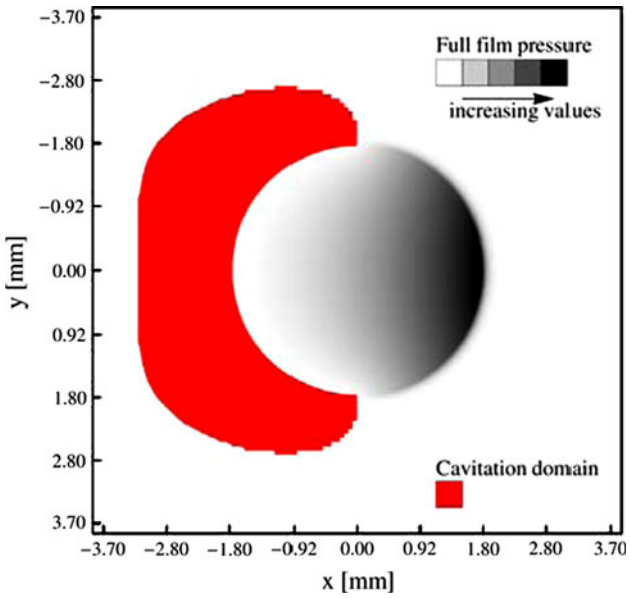

Fig. 6 Fluid pressure field (in *gray scale*, normalized with respect to the maximum calculated pressure value $p_{\max}^{\text{smooth}}$), and the cavitating area (*red domain*) as a function of the contact position, for the same contact parameters adopted in the calculation of Fig. 5b, and for $h_{\min} = 2$ μm (Color figure online)

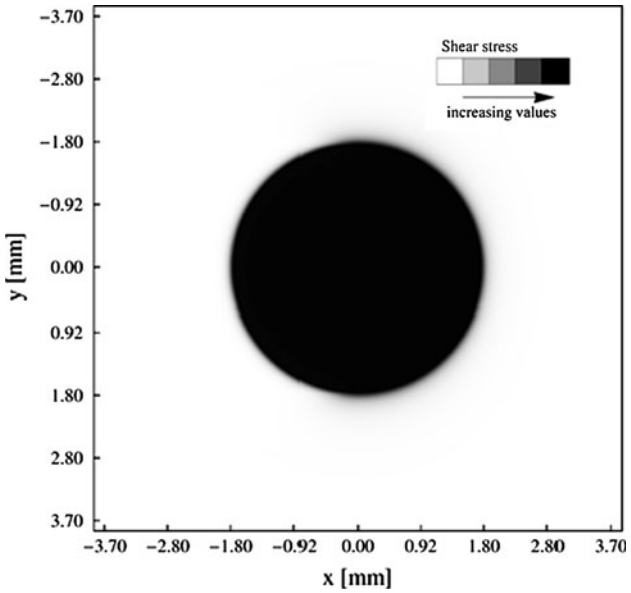

Fig. 7 The frictional shear stress field (in *gray scale*, normalized with respect to the value $\eta U/h_{\min}$), as a function of the contact position

contribution only result from the viscous dissipation in the conforming portion of the domain.

In Fig. 8, we show the COF μ as a function of the product ηU for the control surface case (solid line) and for the microholed textures CT1 ($p_h = 20$ %) and CT2 ($p_h = 35$ %). Very interesting is to observe that the square lattice of holes determines a relevant reduction of friction on the whole range of sliding velocities, i.e., over the entire Stribeck curve, whereas the largest reduction of COF is observed in the hydrodynamic regime with values larger than 50 % compared to the control surface. The density of holes has only a marginal influence in the present case, with a slightly larger friction decrease for CT2 in the boundary-mixed lubrication regime. Moreover, interestingly, both microholed textures do not show any transition to a boundary regime, at least within the investigated velocity range. The fluid pressure field (in gray scale, normalized with respect to $p_{\max}^{\text{smooth}}$), and the cavitating area (red domain) as a function of the contact position, for the same contact parameters of Fig. 6, are show in Fig. 9a, b, respectively, for the texture CT1 and CT2 (note: the hole width w_h has been increased by a factor of 5 in the calculations, while keeping the texture area density. This is not expected, however, to significantly affect the results in the limit $w_h \ll w_d$, where w_d is a representative contact domain length [26]). In this case, the oil film breakdown is

www.manaraa.com

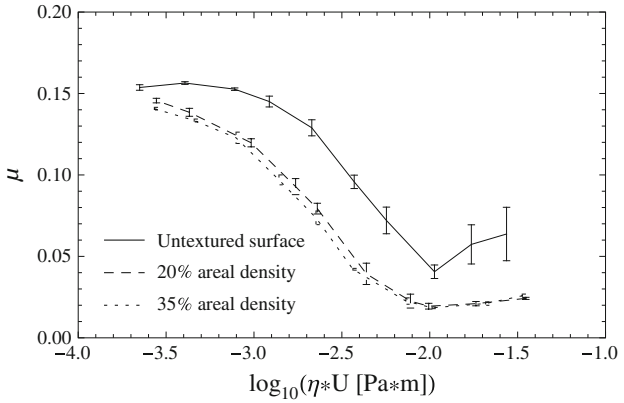

Fig. 8 The coefficient of friction μ as a function of ηU (in a log-linear diagram) for the flat control surface (*solid line*), for the square lattice of microholes with void density 19 % (CT1—*dashed line*), and for the square lattice of microholes with void density 35 % (CT2—*dotted line*). Observe the strong reduction of the COF that is obtained over the entire range of sliding velocities. In particular, compared to the flat control surface, the friction reduction reaches values of about 50 % in the hydrodynamic lubrication regime. Less important is the influence of the microtexture in the boundary and mixed lubrication regimes

predicted in the outlet of the conforming contact domain and, in particular, in correspondence to the texture holes. At the inlet, however, the deterministic roughness pattern only introduces the expected corresponding fluctuation in the fluid pressure solution without basically altering its averaged (over the hole cell length) behavior with respect to the smooth case, see Fig. 6. The frictional shear stress field (in gray scale, normalized with respect to the value $\eta U/h_{\min}$) is instead reported in Fig. 10a, b, respectively for the texture CT1 and CT2. The remarkable friction reduction presented in Fig. 8 can now be related to the average reduction of lubricant shear stresses at the contact interface, which is confined over the texture holes. Indeed, at the contact inlet, where cavitation does not occur, the presence of the holes reduces the fluid velocity gradient (i.e., the shear strain rate) at the location of the dimple without strongly altering the fluid pressure field with respect to the untextured case (scaling with $h_{\min}^{-2}$). As a consequence, the average shear stress (scaling with $h_{\min}^{-1}$) and, hence, the friction force at the interface are reduced with respect to the untextured pair. Moving toward the trailing edge of the contact, lubricant in the microholes cavitates, thus also leading to a reduction of the average wall shear stress.

On the other hand, when the microtexture is constituted by grooves, no beneficial effect in terms of friction is obtained. Indeed, Fig. 11 shows that, in the case of parallel grooves, a strong increase of the friction coefficient μ is observed over the entire velocity range with a maximum increase of 80–100 %. Moreover, the friction increase is larger for the

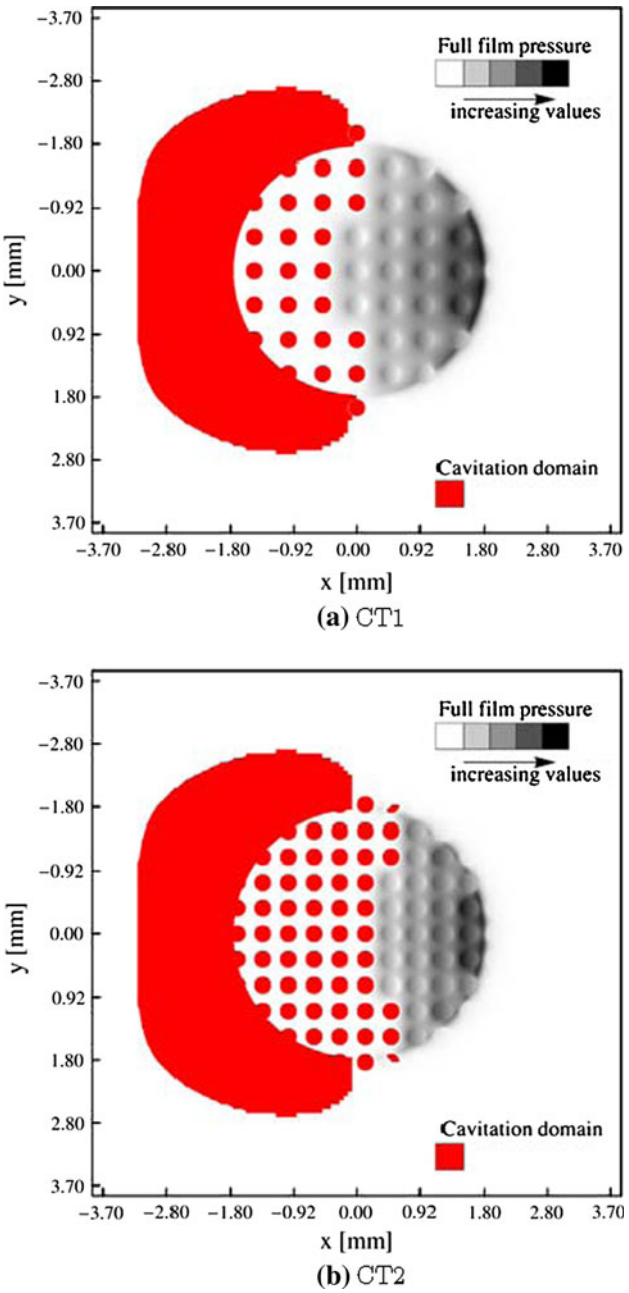

Fig. 9 Fluid pressure field (in *gray scale*, normalized with respect to $p_{\max}^{\text{smooth}}$) and the cavitating area (*red domain*) as a function of the contact position for the same contact parameters of Fig. 6. More then 32 grid points for hole side are used in the calculation (Color figure online)

transverse configuration (GTt—dotted line) than for the longitudinal (GTl—dashed line). We also notice that the transition to the boundary regime is characterized by a decreasing friction as the sliding velocity is decreased. This suggests the occurrence of relevant viscous dissipations at the groove scale which is not accompanied by a corresponding increase of load support capability which, in turn, determines a decrease of the oil film thickness at the

www.manaraa.com

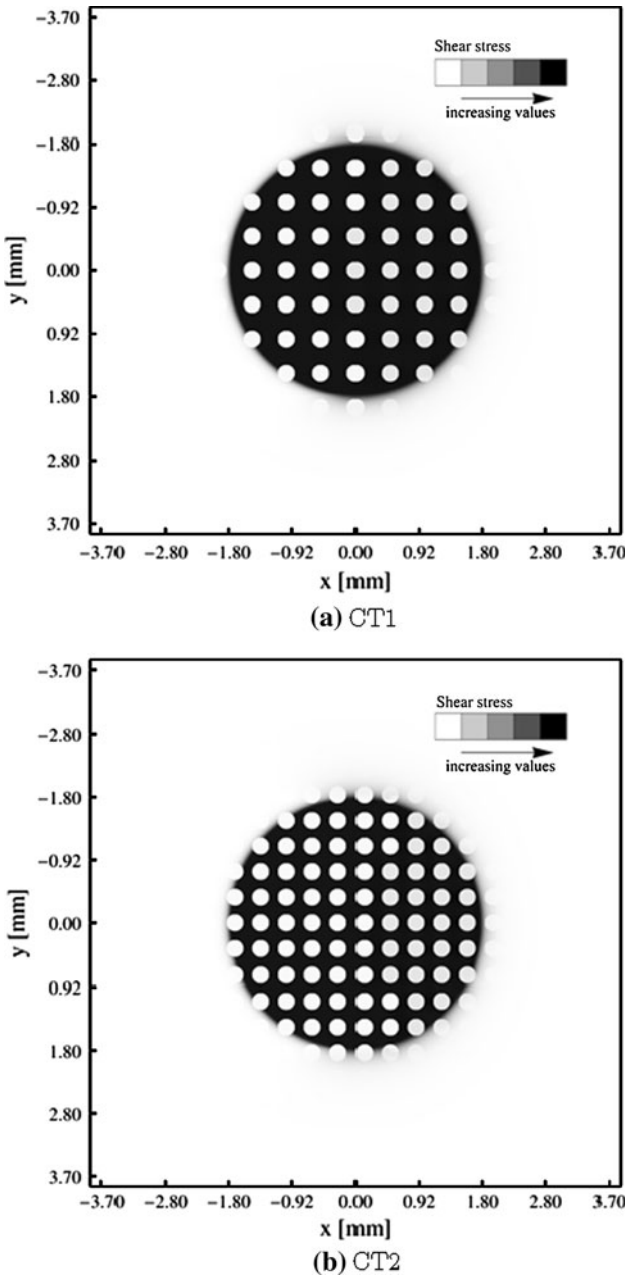

Fig. 10 Frictional shear stress field (in *gray scale*, normalized with respect to the value $\eta U/h_{\min}$) as a function of the contact position, for the same contact parameters of Fig. 6

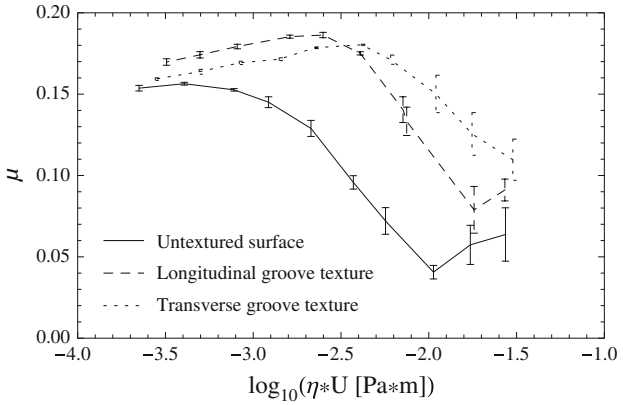

Fig. 11 The coefficient of friction μ as a function of ηU (in a log-linear diagram) for the flat control surface (*solid line*), for the series of parallel grooves aligned with the sliding velocity (GTl—*dashed line*), or disposed perpendicularly to the sliding velocity (GTt—*dotted line*). This time a strong friction increase is observed, which can reach values close to 80–100 % in the mixed lubrication regime. Interestingly, the effect of groove orientation is not really significant although transverse grooves seem to increase further the friction values

interface. In simple words, one may say that parallel grooves do not posses oil trapping properties, as a consequence of a lubricant leakage along the grooves. The previous argumentation is confirmed by the numerical results. In particular, the fluid pressure field (in gray scale, normalized with respect to $p_{\max}^{\text{smooth}}$) and the cavitating area (red domain) as a function of the contact position, for the same contact parameters of Fig. 6, are show in Fig. 12a, b, respectively, for the texture GTt and GTl (note: as before, the groove width has been increased by a factor of 5 in the calculations, while keeping the texture area density). Moreover, the frictional shear stress field (in gray scale, normalized with respect to the value $\eta U/h_{\min}$) is instead reported in Fig. 13a, b, respectively, for the texture GTt and GTl. Observe that the fluid pressure rise at the contact inlet is almost absent for the groove case. In the transverse configuration (Fig. 12a), the fluid leaks out of the contact already at the first groove; whereas, in the longitudinal case (Fig. 12b), the oil flows toward the outlet without undergoing a relevant shearing process (except over the ridges in the immediate contact inlet, where the oil flow has not been yet deviated in the grooves). This negligible viscous action, remarkably, is reflected in the occurrence of a distributed film rupture over the transverse textured surface (Fig. 12a); whereas, in the longitudinal case, a full film is preserved in the whole conforming contact area (Fig. 12b). However, in both cases a negligible pressure rise occurs at the conforming contact, with the result that, in particular for the transverse configuration, the hydrodynamic regime is even completely suppressed (see Fig. 11).

A summary of the previously discussed numerical results is presented in Fig. 14, where we show a cross section over the plane of symmetry of the contact of the dimensionless fluid pressure field. Further investigations are clearly needed to quantify the relevance of the previously discussed results in practical applications, e.g., for the texturing of forming molds. However, the preliminary conclusions reported in the present work show that a proper local microtexturing of the surface can easily control friction and the amount of its increase or decrease.

www.manaraa.com

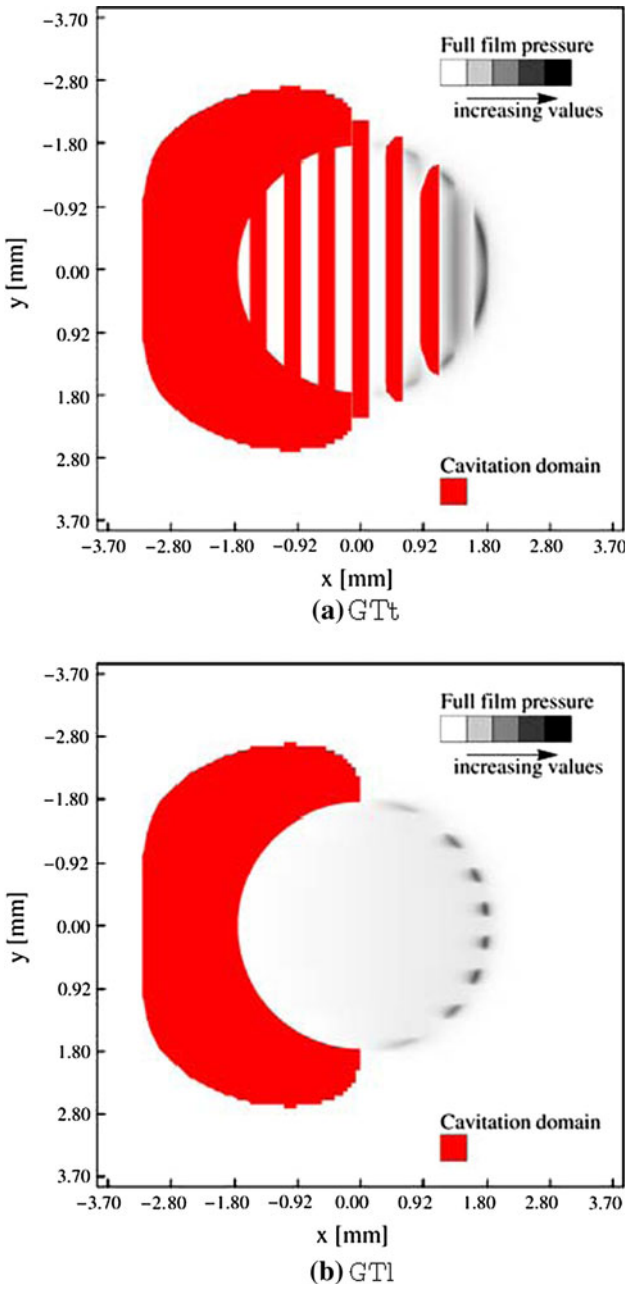

Fig. 12 Fluid pressure field (in *gray scale*, normalized with respect to p_{max}^{smooth}) and the cavitating area (*red domain*) as a function of the contact position for the same contact parameters of Fig. 6 (Color figure online)

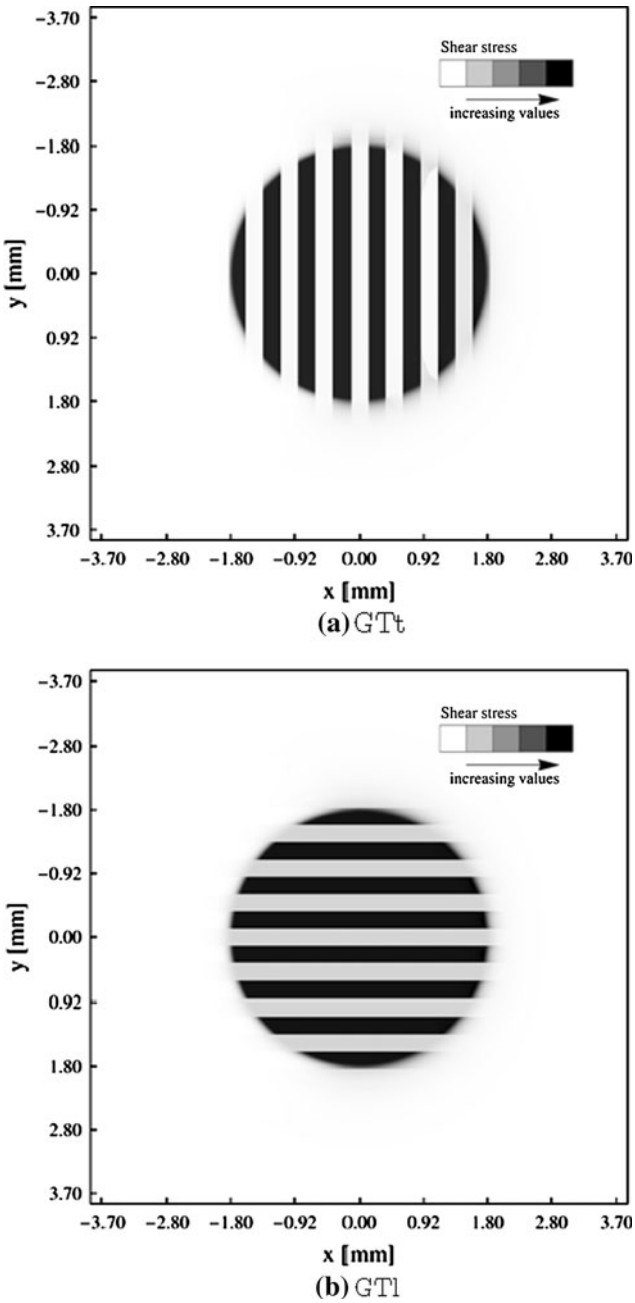

Fig. 13 Frictional shear stress field (in *gray scale*, normalized with respect to the value $\eta U/h_{min}$) as a function of the contact position for the same contact parameters of Fig. 6

4 Conclusions

We have experimentally investigated the frictional behavior of LST surfaces under lubricated conditions. The considered sliding velocity range covers about two order of magnitudes so that almost the entire Stribeck curve has been measured. We have found that depending on the microgeometry of the surface texture, the COF can be accurately controlled. In particular, when the texture consists of a square lattice of microholes, the friction values are strongly reduced over the entire range of lubrication regimes with a maximum reduction of about 50 % in hydrodynamic conditions. A completely different behavior is exhibited when the texture consists of microgrooves. In this case, no trapping behavior occurs; the oil may easily flow along the parallel microducts, leading to a reduction of the mean gap between the sliding surfaces and to an increase of the boundary and mixed lubrication velocity

www.manaraa.com

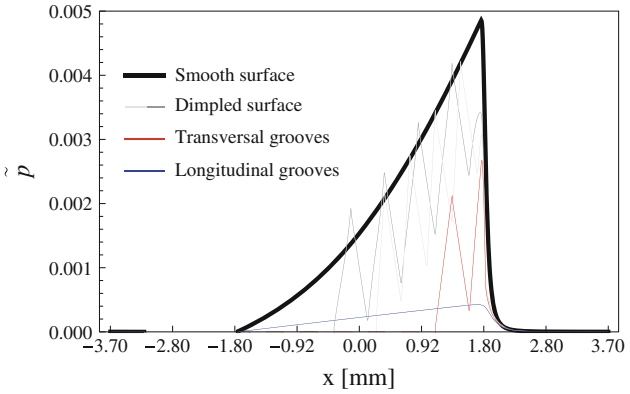

Fig. 14 Dimensionless fluid pressure as a function of contact position (at $y = 0$). For the same contact parameters of Fig. 6, and for the all investigated texture microgeometries (Color figure online)

ranges, followed by a strongly increased friction. Full-scale numerical calculations are also presented and discussed.

Acknowledgments The authors acknowledge Regione Apulia for having supported the research activity through the constitution of the TRASFORMA Laboratory Network cod. 28. The authors acknowledge Dr. D. Sorgente for having incorporated and grinded the ball samples. MS and GC acknowledge Mr. P. Lella, Mr. V. Mele and Mr. G. Olivieri for their invaluable help in preparing the friction experimental setup. The authors finally acknowledge Mr. P. Guastamacchia for his help during the experiments.

References

1. Stratakis, E., Ranella, A., Fotakis, C.: Biomimetic micro/nanostructured functional surfaces for microfluidic and tissue engineering applications. Biomicrofluidics, **5**(1), 13411 (2011)
2. Scaraggi, M., Carbone, G., Persson, B.N.J., Dini, D.: Lubrication in soft rough contacts: a novel homogenized approach. Part I—Theory. Soft Matter **7**(21), 10395–10406 (2011)
3. Scaraggi, M., Carbone, G., Dini, D.: Lubrication in soft rough contacts: a novel homogenized approach. Part II—Discussion. Soft Matter **7**(21), 10407–10416 (2011)
4. Carbone, G., Pierro, E.: Sticky bio-inspired micropillars: finding the best shape. Small **8**(9), 1449–1454 (2012)
5. Carbone, G., Pierro, E., Gorb, S.N.: Origin of the superior adhesive performance of mushroom-shaped microstructured surfaces. Soft Matter **7**, 5545–5552 (2011)
6. Bottiglione, F., Carbone, G., Mangialardi, L., Mantriota, G.: Leakage mechanism in flat seals. J. Appl. Phys. **106**(10), 104902 (2009)
7. Afferrante, L., Carbone, G.: Microstructured superhydrorepellent surfaces: effect of drop pressure on fakir-state stability and apparent contact angles. J. Phys. Condens. Matter **22**(32), 325107 (2010)
8. Etsion, I.: State of the art in laser surface texturing. J. Tribol. **127**(1), 248–253 (2005)
9. Yu, H., Huang, W., Wang, X.: Dimple patterns design for different circumstances. Lubr. Sci. (2011). doi:10.1002/ls.168
10. Scaraggi, M.: Lubrication of textured surfaces: a general theory for flow and shear stress factors. Phys. Rev. E **86**, 026314 (2012)
11. Scaraggi, M.: Textured surface hydrodynamic lubrication: discussion. Tribol. Lett. (2012). doi:10.1007/s11249-012-0025-6
12. Bay, N., Azushima, A., Groche, P., Ishibashi, I., Merklein, M., Morishita, M., Nakamura, T., Schmid, S., Yoshida, M.: Environmentally benign tribo-systems for metal forming. CIRP Ann. Manuf. Technol. **59**, 760–780 (2010)
13. Etsion, I.: Surface texturing. In: Bruce, R.W. (ed.) Handbook of Lubrication and Tribology, Vol. II: Theory and Design, Chap. 53, 2nd edn., pp. 1–16. CRC Press (2012). ISBN 978-1-4200-6909-9
14. Ancona, A., Rãser, F., Rademaker, K., Limpert, J., Nolte, S., Tãnnermann, A.: High speed laser drilling of metals using a high repetition rate, high average power ultrafast fiber CPA system. Opt. Express **16**(12), 8958–8968 (2008)
15. Kovalchenko, A., Ajayi, O., Erdemir, A., Fenske, G., Etsion, I.: The effect of laser surface texturing on transitions in lubrication regimes during unidirectional sliding contact. Tribol. Int. **38**(3), 219–225 (2005)
16. Galda, L., Pawlus, P., Sep, J.: Dimples shape and distribution effect on characteristics of Stribeck curve. Tribol. Int. **42**, 1505–1512 (2009)
17. Vilhena, L.M., Sedlacek, M., Podgornik, B., Vizintin, J., Babnik, A., Mozina, J.: Surface texturing by pulsed Nd:YAG laser. Tribol. Int. **42**(10), 1496–1504 (2009). 13th Nordic Symposium on Tribology (NORDTRIB 2008), Tampere University of Technology, Tampere, Finland, 10–13 June 2008
18. Qiu, Y., Khonsari, M.M.: Experimental investigation of tribological performance of laser textured stainless steel rings. Tribol. Int. **44**(5), 635–644 (2011)
19. Etsion, I., Halperin, G., Brizmer, V., Kligerman, Y.: Experimental investigation of laser surface textured parallel thrust bearings. Tribol. Lett. **17**, 295–300 (2004)
20. Marian, V.G., Gabriel, D., Knoll, G., Filippone, S.: Theoretical and experimental analysis of a laser textured thrust bearing. Tribol. Lett. **44**(3), 335–343 (2011)
21. Etsion, I., Sher, E.: Improving fuel efficiency with laser surface textured piston rings. Tribol. Int. **42**, 542–547 (2009)
22. Yuan, S., Huang, W., Wang, X.: Orientation effects of microgrooves on sliding surfaces. Tribol. Int. **44**(9), 1047–1054 (2011)
23. Adatepe, H., Biyiklioglu, A., Sofuoglu, H.: An experimental investigation on frictional behavior of statically loaded microgrooved journal bearing. Tribol. Int. **44**(12), 1942–1948 (2011)
24. Predescu, A., Pascovici, M.D., Cicone, T., Popescu, C.S., Grigoriu, C., Dragulinescu, D.: Friction evaluation of lubricated laser-textured surfaces. Lubr. Sci. **22**(10), 431–442 (2010). 4th World Tribology Conference, Kyoto, Japan, Sept 2009
25. Ancona, A., Nodop, D., Limpert, J., Nolte, S., Tuennermann, A.: Microdrilling of metals with an inexpensive and compact ultrashort-pulse fiber amplified microchip laser. Appl. Phys. A **94**(1), 19–24 (2009)
26. Pei, S., Ma, S., Xu, H., Wang, F., Zhang, Y.: A multiscale method of modeling surface texture in hydrodynamic regime. Tribol. Int. **44**(12), 1810–1818 (2011)

www.manaraa.com

Reproduced with permission of copyright owner. Further reproduction prohibited without permission.

www.manaraa.com